Cement and Concrete Research 170 (2023) 107180

Contents lists available at ScienceDirect

Cement and Concrete Research

journal homepage: www.elsevier.com/locate/cemconres

Percolation experiment across a 10-year-old interface between Opalinus Clay and Portland concrete

Ellina Bernard [a,b,*], Andreas Jenni [a], Nikolajs Toropovs [c], Urs Mäder [a]

[a] University of Bern, Institute of Geological Sciences, Rock-Water Interaction, 3012 Bern, Switzerland
[b] Department of Civil and Environmental Engineering, Imperial College London, South Kensington, 11 Skempton Building, London SW7 2AZ, UK
[c] Empa, Swiss Federal Laboratories for Materials Science and Technology, Laboratory for Concrete & Construction Chemistry, 8600 Dübendorf, Switzerland

ARTICLE INFO

Keywords:
Portland cement degradation
Opalinus Clay
Saline water
10-year-old interface
Pore solution
X-ray computed tomography

ABSTRACT

An interface sample between Portland concrete and Opalinus Clay with a contact time of 10 years recovered from a field experiment was investigated by SEM-EDX and X-ray CT. The concrete side showed a large chloride ingress from the claystone alongside a decalcification and an opening of the porosity. Additional XRD, TGA and leaching experiments of the concrete at few centimetres (~5 cm) away from the interface confirmed the chloride ingress. The interface was then subjected to a long-term percolation experiment accompanied with repeated X-ray CT-scans. Injection of synthetic claystone pore water proceeded into the claystone-part of the sample, and through the concrete part, whereby the outflow was continuously sampled. The bedding joints that were partially desaturated rapidly saturated, while hydraulic conductivity steadily decreased to values similar to unaltered claystone. The analysis of the exfiltrating aliquots shed light on the advective/diffusive properties of water transport and multi-component solute transport.

1. Introduction

In Switzerland and several other countries, the storage of radioactive waste is planned in deep geological facilities hosted in claystone known for its low permeability and its high sorption capacity favourable to contain radionuclides after breach of containers [1–3]. The safety of these repositories relies on the long-term isolation properties of the engineered barrier system and particularly of the geological environment. Of concern are possible deleterious effects on clay stability, or modification of transport properties (water saturation, gas escape, preferential flow paths, cementation effects). Cementitious materials are an integral part of most repository designs (structural elements) or are present as waste matrix. The hyperalkaline pore waters of cementitious materials and their impact on clay materials (claystone, bentonite) as well as interactions with geosphere pore waters and its impact on cement hydration phases are therefore studied at time scales relevant for the operational phase (10's-100's of years) as well as for an entire service life of a repository (10^4–10^6 years).

A large number of detailed studies on interfaces of claystone (e.g. Opalinus Clay (OPA), Callovo-Oxfordian claystone) from laboratory experiments, in situ tests in underground research laboratories and from natural and man-made analogues provided details mainly on mineralogical alteration in the cement matrix and the adjacent claystone [4–13]. A consortium project studied the interfaces recovered at the Mont Terri rock laboratory (*St.* Ursanne, Switzerland, www.mont-terri.ch) from the Cement-Clay Interaction (CI) Project including different types of concrete, mortars and pastes emplaced in 2007 and in later years.

In addition to the normal hydration of the Portland clinker phases, Portland paste featured a continuous hydration of clinker phases at the interface due to the OPA pore water reservoir [6,8]. The analysis indicated the migration of calcium from the cement across the interface to the cation exchange sites of the OPA, releasing sodium to the OPA pore water, which diffused into the cement. After 3 years of concrete emplacement, portlandite was no longer observed up to ~0.2 mm from the interface, neither was ettringite up to ~1 mm, and there was a complete depletion of C-S-H up to 0.1 mm, while C-S-H content was strongly reduced to 1 mm-depth [6] with a decrease of the Ca/Si in the C-S-H [7]. A relatively large amount of magnesium was observed that precipitated in the OPA a few mm away from the interface [9]. The magnesium enrichment was four times higher than a fully magnesium-exchanged clay matrix [9] and therefore reflected a newly formed solid phase, but not detectable by μ-XRD analysis [6]. Additionally, a carbonated zone was observed in the cement matrix near the interface

* Corresponding author at: University of Bern, Institute of Geological Sciences, Rock-Water Interaction group, 3012 Bern, Switzerland.
E-mail address: ellina.bernard@empa.ch (E. Bernard).

https://doi.org/10.1016/j.cemconres.2023.107180
Received 12 October 2022; Received in revised form 24 February 2023; Accepted 12 April 2023
Available online 29 April 2023
0008-8846/© 2023 The Authors. Published by Elsevier Ltd. This is an open access article under the CC BY license (http://creativecommons.org/licenses/by/4.0/).

and depending on the sample and the distance from the interface, a reduced or an enhanced porosity was detected [9,14].

Studies including pore space characterisation are scarce and are limited by the small size of most pores (micro porosity) present in both materials. Direct evidence of the effect of aged interfaces on transport properties (hydraulic conductivity, effective diffusion coefficients) is still missing. Sound physical, chemical, and hydraulic data are required to model the experimental observations that are now available for up to 10 years of cement-claystone interaction. Understanding the coupled physico-chemical processes may allow for a more reliable modelling prediction.

Experimental devices applying confining pressure with independent control of a hydraulic gradient across a sample provide an excellent way to look at the reactive transport properties of simple or compound samples [15]. In such a percolation experiment of a compound sample containing a material interface, the analysis of the exfiltrating aliquots shed light on the advective/diffusive properties of water transport (traced by deuterium) and multi-component solute transport (anions, cations), the latter being subject to complex mineral reactions and ion-exchange processes. If such an experiment is carried out in X-ray transparent equipment, repeated X-ray computed tomography (CT) over the experimental duration combined with the core infiltration data allows the tracking of the chemical and physical modifications (mineralogy and porosity) both spatially and temporally.

The objective of this work is to perform reactive transport experiments across an aged interface of Portland concrete (PC) and OPA Clay using a new X-ray transparent core infiltration apparatus that allows the monitoring of experiments by repeated CT imaging. The challenges were manifold with respect to equipment design and analytical techniques.

2. Materials and methods

2.1. Description of the core sample subjected to percolation

A well preserved interface between Opalinus Clay and Portland concrete was recovered from the CI Experiment (Cement-Clay Interaction Experiment). This experiment was installed in 2007 at the Mont Terri rock laboratory (*St.* Ursanne, Switzerland, www.mont-terri.ch) to study the chemical, mineralogical, and petrophysical changes at different interfaces between clayey and cementitious materials over time. One focus was on the behaviour of the Opalinus Clay placed in contact with Portland concrete to elucidate the evolution of the interface zone. A detailed description of the set-up and sampling technique [9] includes an overview of results up to five years of cement-clay interaction. The interface between Opalinus Clay and the Portland concrete emplaced in 2007 was sampled in the latest campaign (2017) and chosen for the percolation experiment detailed in this study.

The Opalinus Clay had previously been studied in detail [16]. The OPA, where the CI experiment is located, consists of approximately 62 wt% clay minerals (24 wt% kaolinite, 20 wt% illite, 10 wt% illite/smectite mixed layers, 8 wt% chlorite). Additionally, 20 wt% calcite, 10 wt% quartz, 3 wt% feldspars, 2 wt% siderite, 1 wt% dolomite/ankerite, 1 wt% pyrite, and <1 wt% organic carbon were quantified [9]. The total porosity was averaged to 16 % with a water content of ~6 wt%. The porosity is known to be largely connected and therefore the water content also reflects the total (and connected) porosity.

The concrete was made with Portland cement CEMI 42.5 R HS (238 kg/m^3, chemical composition given in Table 1) with w/c = 0.8 and sand and gravel according to SN EN 12620 (rounded river sediment consisting mainly of limestone, silicate rocks and quartz).

2.2. Estimation of the cement paste chemistry, mineralogy and pore solution after aging

Our sample recovered from the Mont Terri rock laboratory was subjected to the OPA environment during 10 years. The interface region (few first centimetres on either side) is expected to be modified. Further away of the interface, the cement phase assemblage and the in situ pore solution might differ from the phase arrangement of paste samples sealed without OPA pore water. Such samples casted in a laboratory and analysed up to 9 years of aging [9] serve as a reference for chemically isolated systems. Therefore, the chemical characterisation of the interface between OPA and PC but also of the PC matrix at 5 cm distance (see Fig. S 1) from the interface including chemistry, mineralogy and pore solution is necessary to understand physicochemical changes and related mass transfers.

The identification of the hydrates in a concrete is known to be difficult due to dilution effect of cementitious phases, possibly with low crystallinity, in the large amount of aggregates composed of well crystalline minerals. Therefore, the fraction of the cement paste at 5 cm from the interface was enriched by crushing and sieving at 250 μm. The fraction below 250 μm, which is enriched in cement paste, was further ground by hand below a particle size of 63 μm using an agate mortar. The content of remaining aggregate is estimated by X-ray diffraction (XRD) and thermogravimetric analysis (TGA) together with a qualitative assessment of the phase assemblage.

XRD was performed at the University of Bern with a PANalytical X'Pert Pro MPD diffractometer, equipped with a Cu X-ray source and an X'Celerator detector. X'Pert Highscore plus v. 4.6.1. was used for qualitative phase analysis. TGA was carried out at Empa, Dübendorf, using a Mettler Toledo TGA/SDTA 851e under nitrogen atmosphere. Weight loss was measured while heating about 50 mg of sample from 30 to 980 °C with a heating rate of 20 °C per minute in 150 μL alumina crucibles.

Additionally, two samples of 0.6 g of enriched cement paste matrix at 5 cm distance were put in 1.2 mL of $Ca(OH)_2$ saturated solution. After 10 days, the samples were filtrated and analysed by ion chromatography (IC) immediately after filtration. The dissolved concentrations of magnesium, calcium, sodium, potassium, chloride, nitrate and sulphate in undiluted solutions or in solutions diluted by a factor 10 or 100 were quantified using a Dionex DP series ICS-3000 ion chromatography system with a measurement error $\leq$ 10 %. The measured concentrations correspond to the leached ions and back calculations to pore water concentrations is required to estimate the pore solution composition.

2.3. Sample preparation for percolation experiment

To get a well-preserved interface in a 52 mm-diameter core without dislocations, we adopted a similar technique than the one used during field sampling campaigns [9]. Samples from the field were pre-cut and sealed after drilling and kept in cold storage. Further processing consisted of emplacing six parallel fiberglass reinforcements into boreholes arranged circularly (Fig. 1). Two times three boreholes of 8 mm diameter were drilled on a machining mill and filled with 5 mm diameter carbon fibre tubes embedded in Sikadur 52™ epoxy resin. After 3 days, the stabilized 52 mm core was gently dry drilled through the stabilisation pins with a diamond drill bit and air cooling.

Although the sample was well preserved, some partial drying could not be avoided during storage and subsequent sample preparation. During the preparation, the sample was subject to a short pre-wetting event due to an initial leak of the confinement medium, distilled

Table 1
Composition of the Portland cement used in the CI study obtained by XRF.

	SiO_2	Al_2O_3	Fe_2O_3	CaO	MgO	K_2O	Na_2O	SO_3	CO_2	Ref.
CEM I 42.5 R HS	20.6	3.9	5.2	58.8	4.6	0.75	0.27	3.5	1.4	[17]

Fig. 1. Three sides of the core sample just after dry drilling: Concrete above, OPA (dark) below the oblique interface, dark vertical traces of intersected stabilisation pins. Dashed red lines visualise the bedding traces. (For interpretation of the references to colour in this figure legend, the reader is referred to the web version of this article.)

water (uptake in the sample assembly of 1.94 g / <1 wt% of the total core mass). After an initial saturation phase, the transport experiment pertains to a system behaviour in a pore water saturated state (see section 3).

2.4. Set up of the X-ray transparent percolation apparatus

Usually, a compromise has to be made between specimen size (spatial resolution), acceleration of transport (chemical resolution, experimental duration, and large hydraulic gradients), a focus on solid phase characterisation (e.g., X-ray computed tomography) or on recording the mobile phase (e.g., neutron imaging, positron emission tomography).

Most detailed characterisations of the solid phase rely on post mortem analysis, while the internal evolution of the pore network largely remains unresolved. Recent developments in synchrotron techniques also allow highly resolved bulk chemical (μ–XRF, X-ray fluorescence) or mineralogical information (μ–XRD, X-ray diffraction) to be acquired in tomographic mode, but with limits on sample size and experimental duration (beam time).

It is in this context that intermediate-scale laboratory experiments play an important role in bridging scales, by providing relatively highly-resolved information but in a set-up of sufficient complexity and at relevant boundary conditions to be representative of field-scale applications or repository components.

The main parts of the apparatus are a X-ray transparent carbon fibre pressure cylinder (lined with a polymer sheet), a sample core assembly sealed with O-rings, and a construction to hold small pressure containers for confining fluid, infiltration fluid, a sampling syringe and some valves and pressure indicators (Fig. 2). A fluid of the desired composition is injected on one side (bottom) for driving advective flow, and the outflow is collected on the other side (top). The apparatus is designed to fit into X-ray CT scanners, some positron emission tomographs, and to operate self-sustained for several days, e.g. without any connections.

The cylindrical sample (Fig. 1) was mounted between two POM adapters and separated by a PEEK filter fabric with an additional small filter of CFK placed at the inlet and outlet of the PEEK capillary connections (Fig. 3). The adapters and filters were required to distribute and collect the inflow and outflow to and from a sample.

The sample core was isolated from the confining medium (distilled water) by a Teflon membrane (chemical isolation) and an outer latex rubber sleeve (hydraulic barrier). The rubber sleeve was sealed with silicone to the adapter to provide a good initial seal.

The combined assembly of sample and adapters (Fig. 3) was coupled to POM inserts and placed in the X-ray transparent cell (Fig. 2), sealed with O-rings against the carbon fibre cylinder. A spindle is used to adjust

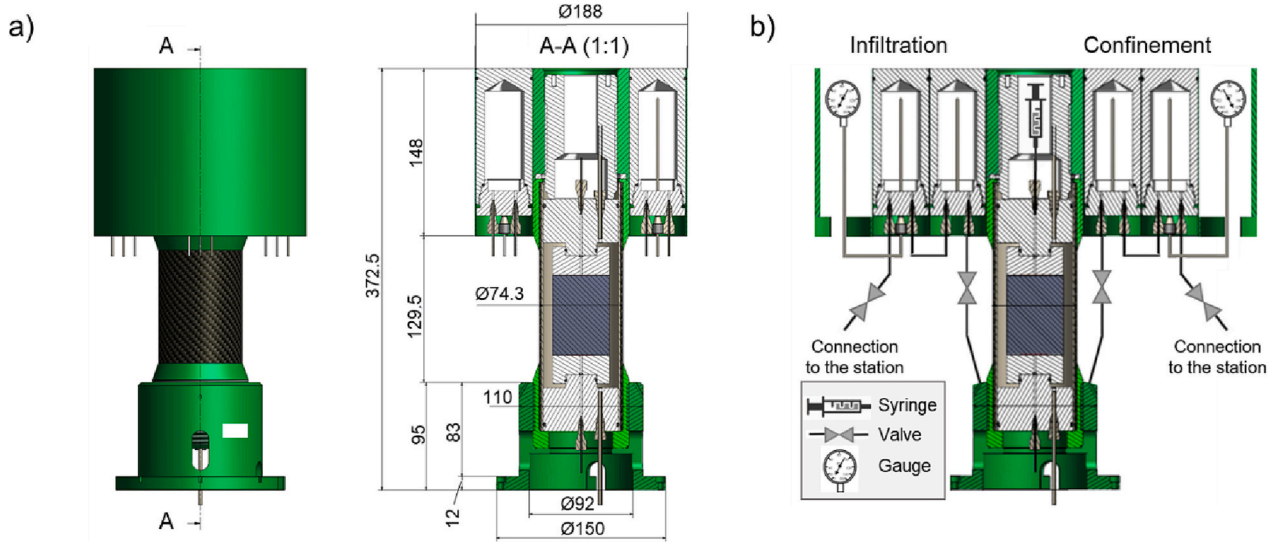

Fig. 2. a) Design of the transparent percolation cell; b) schematic sketch of the transparent percolation cell: its connection to a base station and in an independent mode.

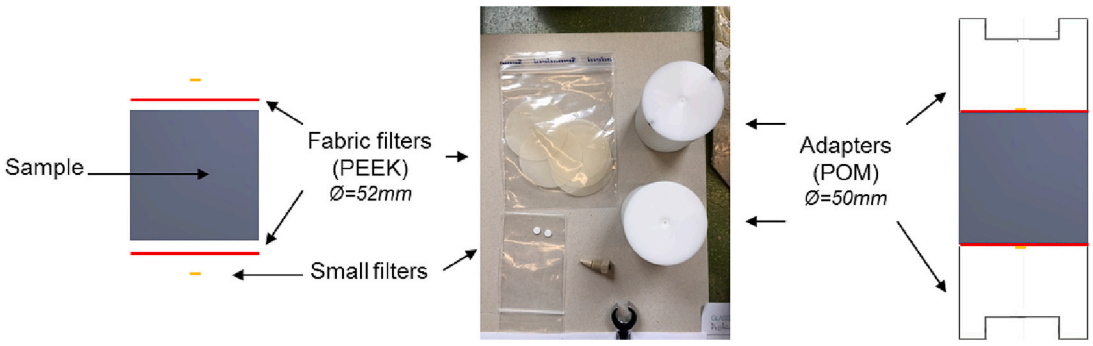

Fig. 3. Schematic of the core sample assembly.

to the length of the core assembly and to provide the axial confinement (fixed length). The system is self-sealing once the confining pressure is stepped up. Pressure is quasi-isostatic, with the axial load somewhat reduced compared to total stress by a small area where the adapters connect to the inserts. The confining pressure is generated in a water/argon separation cylinder that also provides effective compensation for changes in laboratory temperature. PEEK capillary tubes of 1/16" OD (outer diameter) are fed to the surface of the filter and are sealed and held in place by compression fittings. Fluid flow is driven by compressed helium. The mass flow rate is determined at each sampling time, and an accurate hydraulic conductivity can be calculated for the sampling period according to Darcy's law.

Liquid samples were collected at ambient pressure in syringes and this provides a good protection from atmosphere and evaporation. A small back pressure is exerted by the friction of the plunger seal; this friction is approximately known and taken into account in the hydraulic conductivity calculations.

The experiment presented in this study was carried out at room temperature (21–24 °C), slightly higher than the in situ temperature of the CI experiment (13–14 °C). An initial hydraulic head gradient of 40 m/m was applied during 4 months, and then increased to 90 m/m. The injected OPA water was chosen to percolate into the PC as it can be expected that in a repository situation the water will come from the *infinite* host rock towards the cementitious components (hydraulic sink, initially some unsaturated engineered barrier components).

2.5. X-ray CT scanner and image analyses

Computed X-ray tomography (CT) was performed at the University of Fribourg, Department of Geosciences, with a Bruker Skyscan 2211 Multi-Scale nano-CT instrument. Imaging was performed with a flat panel detector (6 Mp). Data were reconstructed with NRecon software optimised for GPU support. A primary data set of projections corresponds to 9.9 GB and a reconstruction of 5.2 GB, voxel size: 30x30x30 μm^3. All the reconstructions were carried out with the same setting for misalignment compensation ($\leq$ 2.5), ring artefact reduction (60) and beam-hardening reduction (50 %). The ring artefacts were prominent and the ring artefact reduction filter during the reconstruction attenuated them, but did not completely remove them. The core was imaged repeatedly at different times to follow the infiltration process, particularly during the early phase of saturation and percolation. Over time, the core slightly shifted in the apparatus. Therefore, the registration of the raw images had to be done with the Elatix plug-in [18] to be able to compare the images over time.

2.6. OPA-PC chemical profiles obtained by scanning electron microscopy (SEM) / energy-dispersive X-ray spectroscopy (EDS)

An analogous sample of the same 10-year-old interface was used as basis for characterising the state before the percolation experiment. Post-percolation data are not yet available because the experiment is still running. The uncoated sample surfaces were examined in a scanning electron microscope (Zeiss EVO-50 XVP) equipped with an EDAX Sapphire light element detector in low vacuum mode (10 Pa) with a beam acceleration of 20 kV and a working distance of 9 mm. The beam current was adjusted to yield a dead time of 10–20 %. Element dispersive spectroscopy maps with 512 × 400 pixels were acquired using a dwell time of 300 µs and 32 or 64 averaged frames. Multiple maps were combined to cover the area of interest, requiring total measurement times of 8–12 h. Higher resolution maps (1024 × 800 pixels), but lower dwell times were used to acquire backscattered electron (BE) images, which depict the average proton number at beam location. Brightness and contrast of the maps were adjusted to reveal gradients within cement or clay matrix, often resulting in oversaturation or undersaturation (in grey-scale) of phases of no interest. Exploring precision of the SEM stage movement, electron beam stability, and image distortion, BE images and smaller maps at higher resolution were also acquired and assembled.

Multiple EDX maps had been acquired in a grid with columns parallel to the interface and rows perpendicular to it. During the acquisition of each map, the EDX detector collected X-rays from the entire map area. The resulting spectra of each map were quantified standardless using a ZAF correction. The quantification of each column of maps parallel to the interface were averaged as in [7]. The averages were plotted as a function of the distance from the interface (chemical profiles across the interface); the range of the different element map quantifications in one column parallel to the interface indicates the chemical variability parallel to the interface, plotted as bars in the figures.

Small areas in the cement or clay matrix were analysed by EDS every 50 µm perpendicular to the interface, avoiding any larger grains (e.g., quartz, calcite, dolomite, pyrite, aggregate) to obtain better resolved chemical profiles. The low-resolution and high-resolution profiles agree well in general for the OPA. The elemental profiles based on large averaged maps show a higher content of calcium, sulphur or iron due to large calcitic bioclasts and pyrite nests heterogeneously distributed, as detailed in [7], which were not measured in the manually defined area measurements avoiding such heterogeneity. Data of averaged element maps from concrete cannot be used due to the large aggregates filling random fractions of each map and masking the cement matrix chemistry. In both standardless quantification approaches, the sum of all elements present is normalised to 100 %, except H, O, and C. Therefore, an absolute decrease of one element concentration is compensated by an increase of all other elements. Porosity, mostly filled by the organic resin, is not part of the quantification.

2.7. Preparation of the artificial Opalinus Clay pore water

A recent NTB [19] summarises the analysis of the Opalinus Clay pore water and gives a composition for relatively undisturbed OPA pore water from exactly this location where also the interface samples were

recovered [20]. This report complemented earlier long-term experiments on the OPA pore water at Mont Terri. Several small aliquots were collected between January and July 2016 from a closed-in sampling interval after 10 years of equilibration time. The measured pH (at 24 °C), alkalinity and ion concentrations are summarised in the SI (Table S1). The alkalinity corresponds to the in situ CO_2 partial pressure of the OPA, but at shallow depth. The calculated speciation (PhreeqC, default TDB) and saturation indices indicate supersaturation of the carbonate minerals due to outgassing of CO_2 and coupled increase in pH during sampling and sample storage.

To keep it simple, the artificial pore water (APW) was back-calculated to calcite-dolomite saturation in equilibrium with the atmospheric CO_2 partial pressure and was only composed of salts (Na^+, K^+, Sr^+, Ca^{2+}, Mg^{2+}, Cl^-, HCO_3^-, SO_4^{2-}). The salts added to Milli-Q water are listed in Table 2 (nominal composition). The composition was modelled with PhreeqC in similar fashion as used for modelling the reference pore water compositions for Nagra's safety case [21]. Finally, δ^2H (^2H_2O) was added to the artificial pore water as a tracer. The chemical analysis of the artificial pore water is presented in section 3.4.

2.8. Analysis of the solutions and the exfiltrating aliquots

After the collection of each syringe sample, the pH was measured in a 50 μL aliquot with a Thermo Scientific™ Orion™ PerpHecT™ ROSS™ combination pH micro electrode, and the rest of the sample was kept in a refrigerator until further analysis.

The samples were analysed for major cations (sodium, potassium, ammonium, calcium, magnesium, strontium) and anions (fluoride, chloride, bromide, nitrate, sulphate) by ion chromatography using a Metrohm ProfIC AnCat MCS IC system with automated 5 μL and 50 μL injection loops. Si and Al were measured only for some samples by ICP-OES on a Varian 720 ES equipped with an autosampler Varian SPS-3 supported by the ICP Expert II Ver. 1.1.2 software and Varian Spectroscopy Database Administrator Ver. 1.6.0.20. Solution samples were diluted with 1 % HNO_3 by a factor of 10 before injection.

Stable isotope analysis of δ^2H and $\delta^{18}O$ were measured by cavity ring-down spectroscopy (CRDS) with a PICARRO instrument, with optimised sample vials to process samples of 0.3–0.5 ml. Data are reported as δ^2H and $\delta^{18}O$ in ‰ relative to VSMOW.

2.9. Calculation of saturation indices

Thermodynamic modelling was carried out using the Gibbs free energy minimisation program GEMS [22] to calculate the saturation indices of the solutions. GEMS is a broad-purpose geochemical modelling code which computes the equilibrium phase assemblage and aqueous electrolyte speciation in a complex chemical system from its total bulk elemental composition. From the measured concentrations in solution and the pH values, the activities of dissolved species were calculated using the geochemical software GEMS v3.7 together with the PSI database [23] and the Cemdata database [24].

The activity of a species i, {i}, is calculated from the measured concentrations considering the formation of different aqueous complexes; {i} = γi·mi, where γi is the activity coefficient and mi is the concentration in mol/kg H2O. The activity coefficients of the aqueous species γi were computed with the built-in extended Debye-Hückel (Truesdell-Jones) equation according to:

$$log\gamma_i = \frac{-A_y z_i^2 \sqrt{I}}{1 + B_y a_i \sqrt{I}} + b_y I \quad (1)$$

where z*i* denotes the charge of species *i*, I the effective molal ionic strength, *by* is a semi-empirical parameter (~0.123 for KOH electrolyte at 25 °C), *ai* = 3.67 Å (for KOH solutions) and A*y* and B*y* are P, T-dependent coefficients. This activity correction is applicable up to ~1 M ionic strength (Merkel and Planer-Friedrich, 2008).

The saturation indices (SI) of the different solids were calculated from the ion activity product (IAP) based on the measured concentrations in the solution according to:

$$SI = log\frac{\mathrm{IAP}}{\mathrm{Kso}} \quad (2)$$

where IAP is the ion activity product and Kso the theoretical solubility product of the solid. A saturation index (SI) < 0 indicates that the solution is undersaturated and the respective solid should not form or will dissolve if present, SI > 0 means that the solution is oversaturated and the formation of the respective solid is possible.

3. Results and discussions

3.1. Description of the 10-year-old interface before the percolation experiment

3.1.1. Physical characterisation of the interface and geometry of the core sample before the percolation experiment

The Opalinus clay – Portland concrete interface was examined with different techniques (Fig. 4): 4a and 4b are reflected light and the BE images obtained on the dry and resin-embedded samples prepared for SEM, while 4c and 4d show two reconstructed X-ray CT images (transversal and orthogonal) of the core before starting the percolation experiment. Both were collected from the same interface, a few centimetres apart from each other. The fabric of the concrete can be observed by both techniques: macropores (black), aggregates (rounded features), and paste in between them. The OPA presents a more homogeneous matrix with jointing parallel to bedding and. Oblique to the interface (4b and 4c). Shrinkage cracks with distinct apertures (BE images, 4a and 4b) seen in dried samples may reflect features originating from a narrow drilling-disturbed zone. Such a fracture was also observed in the reconstructed X-ray CT images (Fig. 4 c and d) cross-cutting jointing, but it is less prominent due to the absence of complete desiccation. The intensity of the bedding-parallel jointing pattern varies at the field-scale and relates to the formation-internal regional deformation history [25]. Bright specks represent small inclusions of phases with very high X-ray attenuation, such as pyrite in the OPA. The sample preparation of the original interface sample and that in the laboratory for the percolation experiment did not result in further disturbances but preserved this fractured aspect well. Because the joints have no significant apertures, the hydraulic effect may be small or only initially be significant compared to intact OPA.

Segmentation of reconstructed X-ray CT images for further volumetric analysis and visualization were performed with Fiji software. Due to the geometry of the core and the resolution of the reconstructed X-ray CT images, only the macro porosity can be accessed, i.e. porosity larger than 60 μm (2 times the voxel dimension). Six segmented sub-volumes are visualised in Fig. 5, where a) corresponds to grayscale 8bit rendered data; b) visualisation of segmented volumes: b1 – large aggregates, b2 – paste intermixed with the smallest sand fraction, b3 – Opalinus clay, b4 – gas pores, b5 – regions of higher porosity close to interface within the cement paste matrix, b6 – damaged interfacial volume at the interface between OPA and PC, and c) represents the sum

Table 2
Salts (PA-grade) used for the artificial pore water.

	NaCl	$NaHCO_3$	$CaCl_2{\cdot}2H_2O$	KCl	$MgCl_2{\cdot}6H_2O$	Na_2SO_4	$SrCl_2{\cdot}6H_2O$	^2H_2O
g/L	12.393	0.044	2.134	0.108	3.337	2.018	0.131	~ 0.035

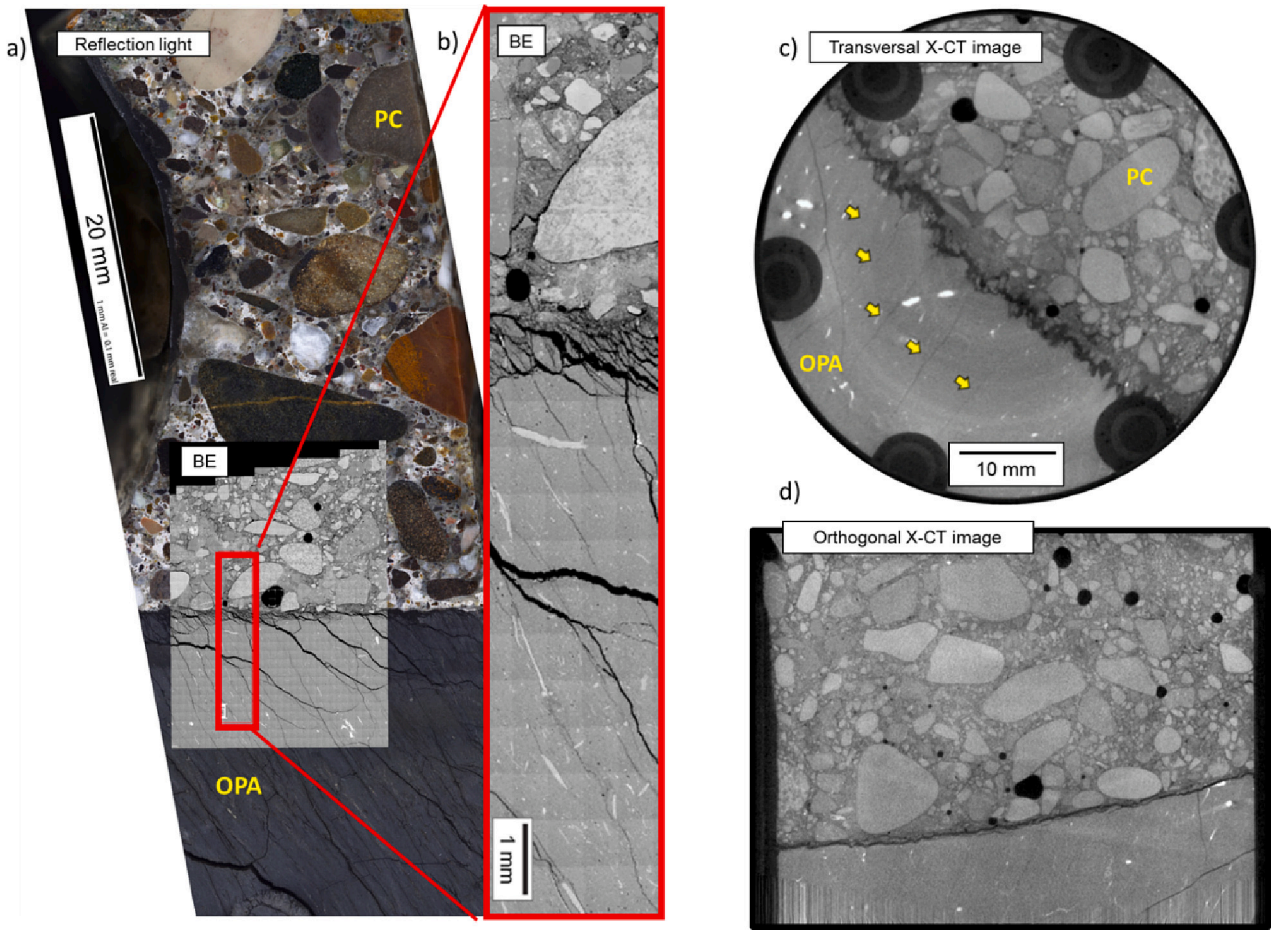

Fig. 4. a) Reflected light and the BE maps obtained on the dried and embedded sample prepared for SEM/EDS, b) zoom of the BE map; sections of the reconstructed X-ray CT data c) transversal and d) orthogonal of the core before the percolation experiment. Both are from the same interface separated by only a few centimetres.

of the segmented sub-volumes. Based on segmentation and extrapolation of corresponding results to core size (μCT was performed on a region around the interface between OPA and PC to increase resolution), the following volumes were calculated (see Table 3). The percentage of aggregate, paste and small sand particle and air void in the concrete were estimated to 57, 42 and 1 vol%, respectively. The obtained content of paste is higher than in the bulk concrete mix used (estimated around 20–25 vol%), and this might be because we cannot resolve the finest sand in the paste, and because large aggregates were not statistically represented close to the interface during the emplacement (wall effect).

3.1.2. Chemical analysis of the interface after 10 years

The SEM/EDS profiles (Fig. 6) from an interface sample neighbouring the sample used for the percolation experiment (see Fig. 4) reflect the alterations that formed over the past 10 years at the interface between the OPA and the cement paste excluding the aggregate in the concrete (as detailed in *2.6*).

The bulk chemical composition of the Portland clinker calculated from the XRF analyses (from Table 1) is shown at the very left in Fig. 6. Few millimetres away from the interface (~ 5 mm), the chemistry in hydrated PC paste is expected to be unaffected by OPA interaction. However, we observe an in situ composition with a calcium content of about 45 mol% instead of 60 mol% in the bulk further away, silicon of 30 mol% instead of 20 mol% and aluminium of 7 mol% instead 4.5 mol %. As detailed previously in [8], the content of Mg is rather high for a normal PC composition, about 5 ± 2 mol% with a large scatter, and the content of sulphate is higher than the initial content (> 2 mol%). This is in agreement with the presence of portlandite, ettringite, C-S-H and hydrotalcite observed by XRD and TGA in the cement matrix but the disturbance due to interaction with OPA is actually wider than the 4-mm-width investigated (limit of sample examination, TGA and XRD at 5 cm are shown in SI).

To document the compositional change at the interface excluding porosity, Fig. 7a and b image the Al/Si, K/Si, Na/Si ratios vs. Ca/Al close to the interface, based on the chemistry given in Fig. 6, segmented for the first 4 mm. The lightly coloured circles correspond to the measurements within the first millimetre while the diamonds correspond to the measurements between 1 and 2.5 mm from the interface, and the dark squares to the ones measured between 2.5 and 4 mm.

Within the first mm, strong differences in chemical composition were detected. The cement paste at the interface contained less calcium (20 mol% compared to 60 mol% in the unaltered cement paste), while increases of silicon (from 20 mol% to 42 mol%) and aluminium (from 4.5 mol% to 20 mol%) were observed. The calcium-depleted zone at the interface is much wider (> 5 mm) compared to that after 4.9 years of interaction (0.1–0.3 mm) [9]. This Ca depletion was caused by the dissolution of cement hydrates up to different depths (portlandite, ettringite and C-S-H) and subsequent calcium diffusion into OPA [6]. The large difference to the 0.1–0.3 mm observed after 4.9 years might be due to a different geometrical configuration of the boreholes, but mostly due to a difference in porosity between the two samples (0.35 after 4.9 years) which lead to a different behaviour in the long term. The increases of silicon and aluminium are explained by compensation of the Ca depletion within the standardless quantification method and does not necessarily indicate in-diffusion from the OPA (see section 2.6). However, the latter cannot be excluded, accompanied by Si and Al uptake in

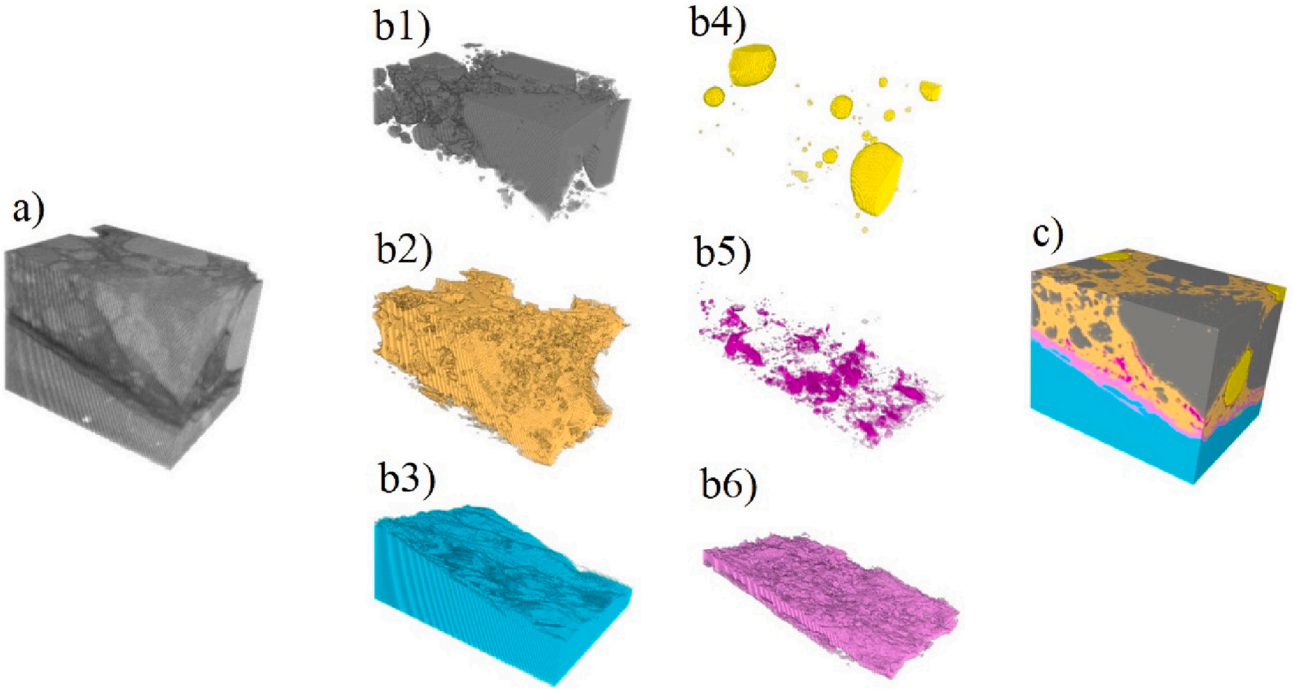

Fig. 5. Visualization of tomography data, a) grayscale 8bit rendered data; b) visualization of segmented volumes: b1 – aggregates, b2 – paste, b3 – Opalinus Clay, b4 – gas pores, b5 – regions of lower porosity close to interface, b6 – interfacial volume between OPA and PC; c) represents the sum of the segmented sub-volumes. Dimension of block: 8.0 × 8.9 × 7.5 mm^3. (For interpretation of the references to colour in this figure, the reader is referred to the web version of this article.)

Table 3
Dimensions and volumetric characteristics of the Portland concrete/Opalinus Clay interface core.

	Core	Opalinus Clay	Portland concrete				Interfacial zone
			Total	Aggregate	Paste	Gas void	
Averaged thickness (mm)	49.1	20.4	28.6				
Diameter (mm)	51.9						
Volume (calculated from μCT) (cm^3)	90.48	35.17	54.47	31.1	22.76	0.70	0.84

C-S-H. The source of Al and Si from OPA is not the pore water itself (e.g. very low *Al* concentrations), but likely some small amount of *Al*-silicate dissolution (clays, feldspars) right at the interface under elevated pH conditions.

The content of sodium in the cement paste at the interface was measured to be higher than in the reference PC content: about 1–2 mol% instead of 0.5 mol%. Similarly to Na, the content of potassium was elevated at the interface (3 mol%) and decreased below 0.5 mol% further away, lower than the reference PC content (1 mol%) (see Fig. 6c). Chloride uptake in the cement from the OPA pore water behaved differently; usually below EDS detection in PC, it increased gradually from the interface (~ 0.5 mol%) up to 2 mol% at 4 mm distance. S was depleted at the interface, but increased (up to 7 mol%) ~2 mm away from the interface and decreased further away towards the initial content of ~2 mol% (Fig. 6b). This might be related to the low pH at the interface where neither SO4-AFm nor ettringite are stable. A slightly higher pH at ~2 mm accompanied by SO_4 lead to precipitation of SO_4-AFm or ettringite.

The sulphate and especially the high Na and Cl present in the OPA pore water (see *3.4.2. Extracted aliquots*) migrated into the concrete and possibly precipitated (see below). The K is rather low in the OPA pore water but it is present in the illite and would be available on partial dissolution as postulated above for supplying Al and Si.

The ratios Al/Si, K/Si and Na/Si vs. Ca/Al close to the interface (light circles in Fig. 7a and b) confirm the generally elevated contents of Al, K, and Na vs. a decreased Ca content. Interestingly, the Al/Si and K/Si display the same trends, although not the same slopes (Fig. 7a and b). This might indicate the additional precipitation of a phase containing Al and K, and supposedly with Si as in C-A-S-H and/or hydrated alkali-alumino-silicate, such as a precursor of zeolite phases [26]. The content of Na was also higher close to the interface as detailed above, certainly due to the high concentration of NaCl in the OPA pore water, its diffusion into the concrete, and the uptake of Na replacing some of the K in hydrates such as C-S-H [27].

The behaviour of Cl was different, while the Cl ingress was much deeper into the concrete only little Cl was observed at the very interface. Cl possibly replaced OH in the AFm (Friedel's or Kuzel's salt) [28] and hydrotalcite phases [29]. Fig. 7c displays the Cl/Al and SO_4/Al ratios vs. Ca/Al and shows a linear trend between Cl and Ca, and between SO_4 and Ca, that correlates with the incorporation of Cl and SO_4 in AFm phases i.e. in mono sulphate phases, Friedel's salt, Kuzel's salt or possibly in hydrotalcite. Possibly, the Cl can be sorbed at the surface of C-S-H or more precisely can compensate the positive apparent surface charge in its diffuse layer [30] and Cl/Si ratios in C-S-H up to ~0.2–0.3 were observed by SEM/EDX [29,31]. The positive apparent surface charge occurs in C-S-H with a high Ca/Si [32–34]. This could explain why the uptake of Cl is lower at the interface where C-S-H are decalcified (i.e. presenting low Ca/Si) than further away from the interface where the less altered paste is present with high Ca/Si C-S-H.

The OPA is weakly altered compared to the PC concrete. This can be explained by the lower porosity and diffusion coefficient in OPA which minimise the mass transfer needed for precipitation in OPA.

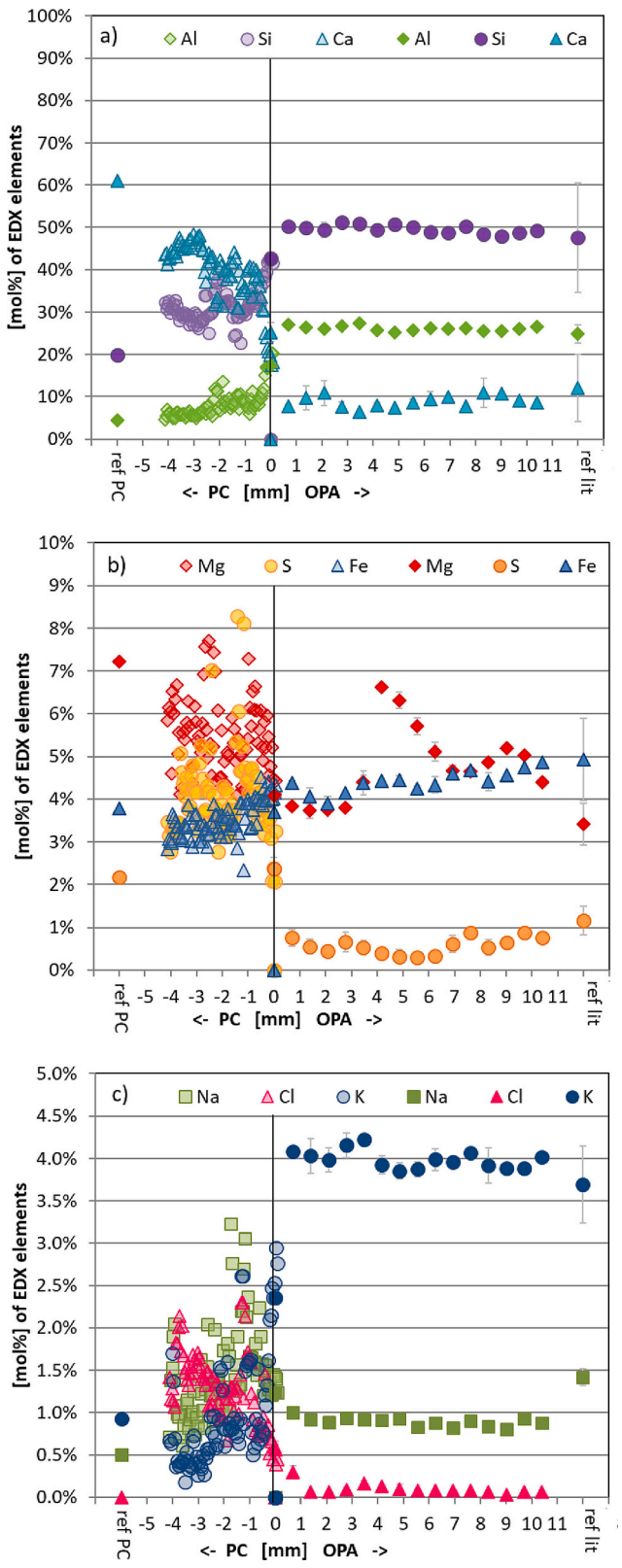

Fig. 6. Element concentration profiles determined by EDS across the interface Portland paste in contact with OPA after 10 years. Dark symbols show the average composition of an area (see 2.2) while the light symbols correspond to surface spot measurements chosen by hand in the homogeneous matrix close to the interface. (For interpretation of the references to colour in this figure, the reader is referred to the web version of this article.)

Additionally, the clay minerals of the OPA show extremely slow dissolution kinetics, and abundant calcite and quartz are rather stable.

3.2. Physical changes in the core during the percolation probed by X-CT

As detailed above, some partial drying could not be avoided during storage and subsequent sample preparation. The joints parallel to bedding seen on the reconstructed X-ray CT images (Figs. 4c, 8) disappeared shortly after starting the infiltration (Fig. 8, after 25 h). This indicates that the OPA is particularly sensitive to partial drying and enhancing jointing, but relatively fast swelling is closing the very small apertures during resaturation. This is direct evidence for the self-sealing ability attributed to OPA. In contrast, an oblique fracture (Fig. 8, left side) that relates to artefacts of the original borehole disturbed zone (see Section 3.1.1) or to sample preparation remains open for much longer, but does not connect from base to top and therefore is not hydraulically active.

Segmentation and quantification of the joint system was not possible due to the very small apertures. To evaluate the more pronounced changes in the core over time, the interface region (Fig. 5, b6) between OPA and PC with air voids (Fig. 5, b4) and zones of elevated porosity (Fig. 5, b5) close to the interface were extracted from the core sample (Fig. 9, a) and processed as a function of time. OPA and PC are presented in original grey scale of X-ray attenuation (Fig. 9a) as reconstructed from the X-CT data. Three time steps (Fig. 9b, c, d) correspond to the same block, where (b) is the reference (initial) state, (c) documents changes after 25 h and (d) after 111 days. The colour mapping documents relative changes and is identical for all snap shots, and it is normalised, where 0 is set as the state at $t = 0$ for the region of interest (see Fig. 9b). To obtain the evolution over time, the initial state of the interface zone and air voids were subtracted from subsequent measurements in 8-bit grayscale values. The colour scale bar "physics" from Fiji lookup tables was used to present the changes, where 0 (blue) corresponds to initial state, while 1 (red) is set at maximum changes between 0 and 111 days. In all cases, the changes correspond to a brightening of voxels, interpreted as an increase in water saturation, displacing initially gas-filled void space. The main changes (red) were located in the air void region while the porous interface zone underwent less change. The interface zone appears to already have contained some pore solution or low density gels and thus only limited changes were observed by X-CT.

3.3. Transport properties

3.3.1. Darcy's law

The bulk hydraulic conductivity of the core sample along its cylindrical axis can be calculated according to Darcy's law, simplified for one dimension:

$$q = \frac{Q}{A} = K\frac{\Delta h}{l} \tag{3}$$

With:

q = specific discharge (m/s) or specific flux ($m^3/m^2/s$)
K = hydraulic conductivity (m/s)
Q = average volumetric flow rate (m^3/s)
l = length of sample (m)
A = cross sectional area of sample (m^2)
Δh = average hydraulic head difference (m water column);

Knowing the bulk conductivity, a back-analysis of the hydraulic conductivity of the perturbed interface can be calculated knowing or assuming a range of values for the individual properties of the Opalinus Clay and Portland concrete involved. Darcy's law can be generalized for a layered medium (perpendicular to the flow direction), using the hydraulic resistivities of the individual layers of thickness l_i, $R_i = l_i/K_i$ in Eq. (4).

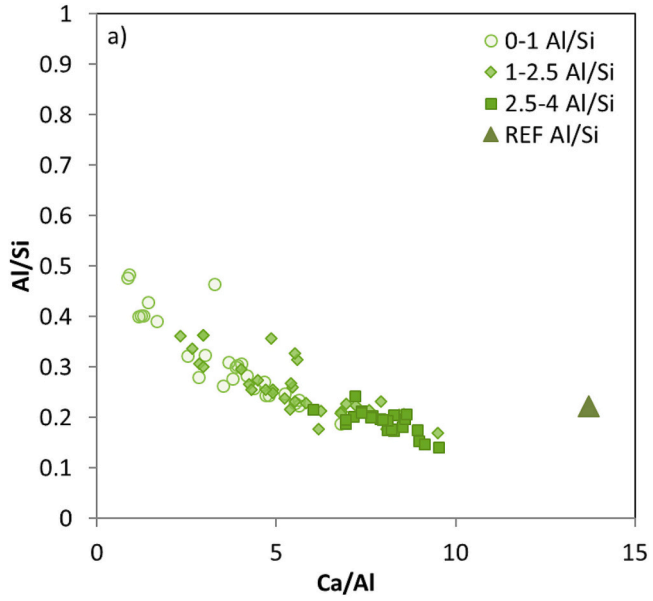

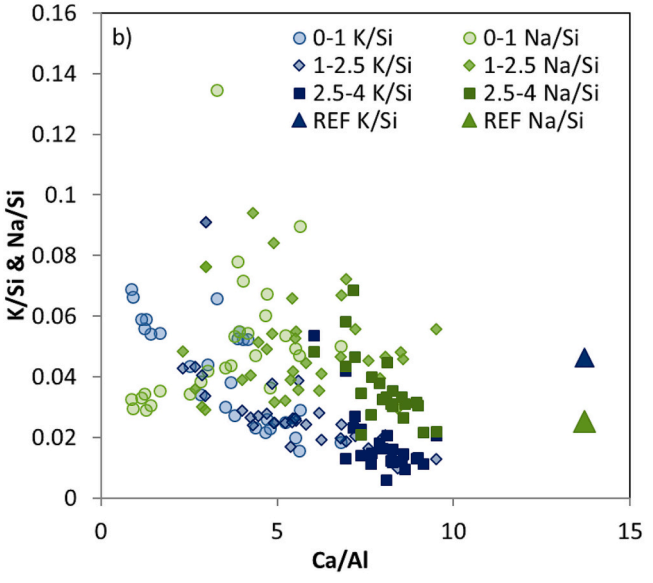

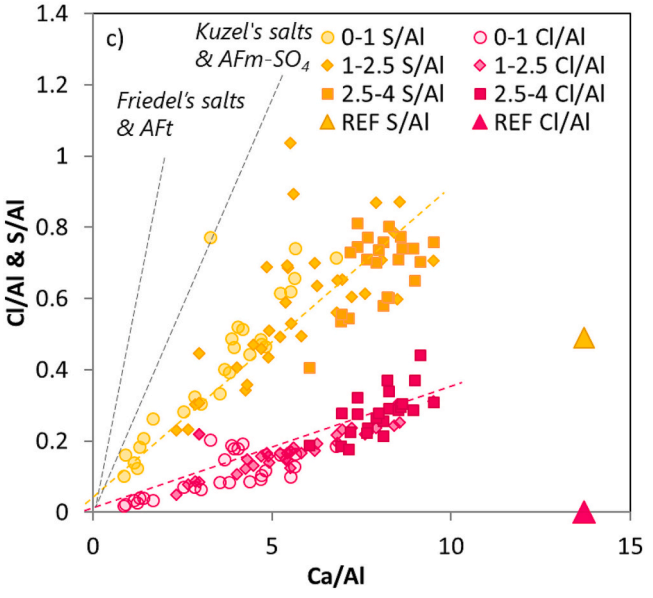

(caption on next column)

Fig. 7. a) Al/Si molar ratio vs. the Ca/Al molar ratio b) K/Si and Na/Si molar ratios vs. the Ca/Al molar ratio c) Cl/Al and S/Al molar ratios vs. the Ca/Al molar ratio from the surface spot measurements chosen manually in the homogeneous matrix close to the interface from Fig. 6. "REF" values correspond to the bulk ratio for the reference composition of the PC cement. Categories relate to distance range [mm] from the interface.

$$q = \frac{\Delta h}{\sum_i R_i} \tag{4}$$

For a three-layer medium, such as the core used in this experiment, consisting of Opalinus Clay, Portland concrete and an alteration zone (skin), one may write:

$$q = \frac{\Delta h}{\frac{l_{PC}}{K_{PC}} + \frac{l_{skin}}{K_{skin}} + \frac{l_{OPA}}{K_{OPA}}} \tag{5}$$

It is evident in the above equation that layers of low hydraulic conductivity and a relatively large thickness are dominant in controlling the flux. Portland concrete with a hydraulic conductivity much larger than Opalinus Clay bears little weight in the Eq. (5). A skin can only be hydraulically effective (detectable) if its hydraulic resistance is similar or larger than that of the OPA layer. Given the small thickness of the skin (mm), its hydraulic conductivity needs to be correspondingly much smaller to be detectable in such an experiment, by a factor of 10–20 at least. Results are presented further below.

3.3.2. Porosity evaluation and transport properties of the OPA and Portland concrete

The porosity in the OPA is well known [35], about 16 % for the shaley facies (mostly micro and nano porosity). Hydraulic conductivity of the Opalinus Clay from Mont Terri has been widely studied and depends on sample lithology and possibly also on sample preparation and the experimental approach. A range of $3{\cdot}10^{-15}$ to $5{\cdot}10^{-13}$ m/s is reported by [16]. More appropriate is a well constrained value of $1.3{\cdot}10^{-13}$ m/s experimentally measured perpendicular to bedding [15] over a period of 15 years on a sample from the same facies and from very near the location of the CI experiment. A recommended average value for the shaley facies from the latest summary is nearly identical, $2.0{\cdot}10^{-13}$ m/s [35], also meant for an orientation perpendicular to bedding. The anisotropy ratio (parallel/perpendicular to bedding) is approximately 5 for a water tracer like HTO for the effective diffusion coefficients [36], but is experimentally not well constrained for hydraulic conductivity. It is most likely that also the hydraulic conductivity is significantly larger parallel to bedding compared to a direction perpendicular to it.

The porosity of fresh concrete depends mainly on the two factors, w/c and degree of hydration [37]. In the case of our specific concrete, the w/c was very high (0.8) but the degree of reaction continuously increased due to water supply provided by the OPA [8]. Thermodynamic modelling of the hydration of PC paste in a closed system (detailed in SI, Fig. S 3) results in a porosity between 45 and 60 vol%, representative for cement matrix not affected by interaction with OPA. The permeability in concrete depends mainly on its capillary porosity [38]. Comparable Portland pastes and mortars aged for 2 years and with a low w/c of 0.47 yielded values between $9{\cdot}10^{-11}$ m/s (mortar) and $2{\cdot}10^{-10}$ m/s (paste) [39]. The PC in question can be expected to be significantly more conductive due to its much higher w/c.

The paste close to the interface is less dense as seen in X-CT data (see Fig. 5, b5), indicating continuous leaching of the paste and generation of additional porosity due to the in-situ interaction during the past 10 years. Similarly, but with a more pronounced increased porosity is the interfacial zone compared to the OPA and also to the paste of the concrete. There is no independent information of the hydraulic conductivity across the interfacial zone. From the above analysis it follows that the bulk hydraulic conductivity is dominated by the OPA (Eq. (5)).

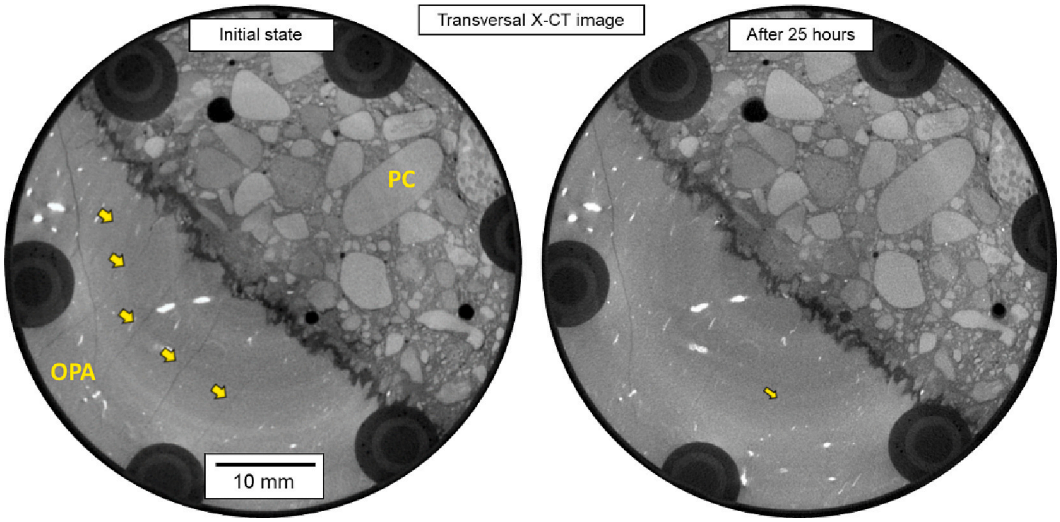

Fig. 8. Reconstructed X-ray CT data of the same transversal section of the core a) before the percolation experiment and b) after 25 h of fluid infiltration. The arrows indicate joints that close shortly after infiltration.

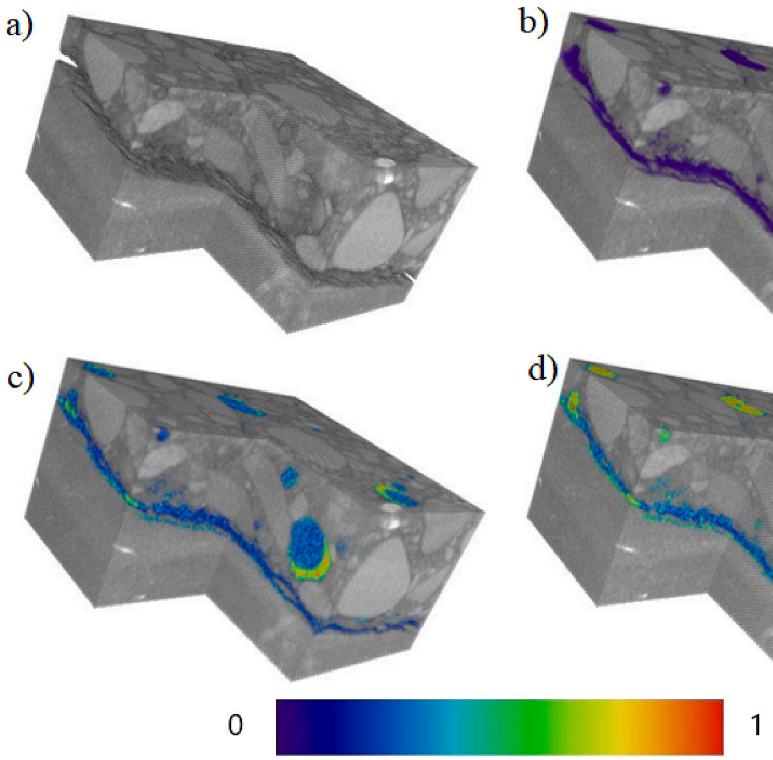

Fig. 9. Graphical rendering of a time series for the interface region. OPA and PC solids are in grey scale, interface zone and air voids are in colour. a) - OPA and PC with voids and interface zone removed; b) t = 0; c) $t = 25$ h; d) $t = 111$ days. Colour scale indicates relative changes (0: initial state b, 1: largest change found after 111 days in d). Dimensions of block. 16.8 × 15.9 × 9.0 mm^3. (For interpretation of the references to colour in this figure legend, the reader is referred to the web version of this article.)

The interface sample expelled gas during the first 2 weeks of percolation, and at least 20 mL was quantified from the exfiltrating aliquots. This volume is the sum of unsaturated porosity in the core, entrapped air in the experimental set-up, and any gas produced during the experiment. Gas production (microbially induced processes, small amounts of dissolved He from the percolation solution, seepage of Ar used in the confining medium) is not known, such that we cannot calculate the initially unsaturated volume of the core.

3.3.3. *Evolution of hydraulic conductivity with time*

The measured hydraulic conductivities of the bulk core were calculated from the incremental solution mass (only liquid) recovered over time, the core dimensions and the average hydraulic head difference for a given sampling interval (Fig. 10, Eq. (3)). The hydraulic conductivity reached $\sim 1.8 \cdot 10^{-11}$ m/s during the first two days. It decreased to $7 \cdot 10^{-12}$ m/s after 10 days, and more slowly to $2.5 \cdot 10^{-12}$ m/s after 116 days. This is about one order of magnitude larger compared to a sample of reference OPA only ($2.0 \cdot 10^{-13}$ m/s), oriented perpendicular to bedding. The limiting value for the tested OPA segment ($l_{OPA}/l_{core} = 0.4$, Table 2) is $\sim 1 \cdot 10^{-12}$ m/s assuming infinite conductivity for the PC and interface. This is still a factor of 5 smaller compared to an intact sample of shaley facies oriented perpendicular to bedding. Our sample is oriented oblique to bedding, with bedding traces intersecting both the inlet surface of the core as well as the interface (Figs. 1 and 4c). A significant part of the apparent elevated hydraulic conductivity at later times may therefore be due to the orientation effect of bedding and only to a limited

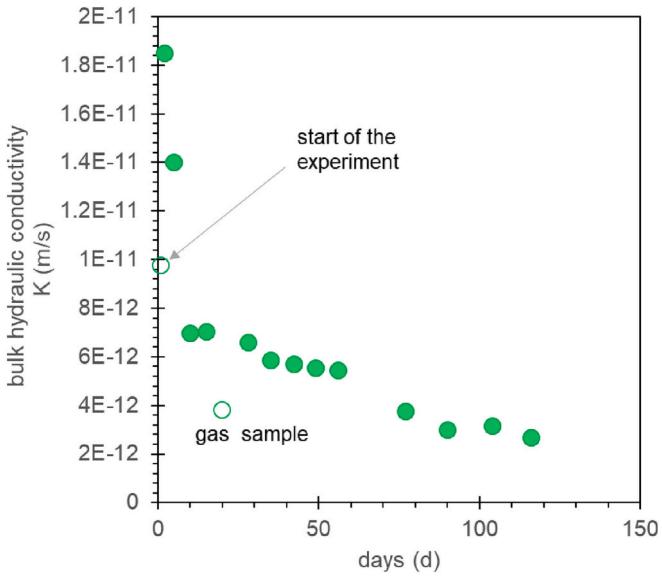

Fig. 10. Bulk hydraulic conductivities (at laboratory temperature, ~ 21–22 °C) calculated from the aliquots; gas sample corresponds to the sample used for gas analysis, in this case, the small back pressure exerted by the friction of the plunger seal in the gas syringe is not known and no correction has been made.

extent to persisting but gradually decreasing preferential flow along bedding-parallel joints.

The strongly elevated hydraulic conductivities during the first few days reflect rapid advection along the initially desaturated joint system across the OPA and past the interfacial zone into PC and out to sampling. The true fluxes (at the inlet) were even higher because of the displaced gas that was not considered in the evaluation. X-CT imaging indicated that the joints largely closed during the first day, but the flux data indicated that this early reduction of hydraulic conductivity lasted about a week. It may well be that only the hydraulic changes in OPA were the determining factor for the composite core, and that the PC with its much higher conductivity played an entirely passive role. The later phase of linearly decreasing conductivity may indicate the existence of some decreasing preferential flow along the closing joint system, but transport is becoming increasingly diffusion-dominated at these relatively low average groundwater velocities. This overall behaviour indicated that self-sealing of desaturated fractures / joint systems was initially rather rapid, but self-healing (complete sealing) was requiring more time.

A similar experiment with an interface of OPA and low-pH mortar where bedding in the OPA was perpendicular to the flow [40] showed a positive skin effect of the interfacial zone with a reduced conductivity [41] compared to a reference value for OPA [35]. However, in the present study the presence of a skin at the interfacial zone could not be demonstrated mainly due to the lack of reliable conductivity data for a sample of reference OPA oriented oblique to bedding. The relatively low X-ray absorbance of the interface region (Figs. 8, 9) is more indicative of being more porous than OPA, and thus also more transmissive.

3.4. Chemical evolutions in the percolating system

3.4.1. Opalinus Clay artificial pore water

The measured composition of the injected Opalinus Clay artificial pore water (Table 4) has a slightly higher NaCl content than measured from in-situ sampling (see SI, by~4–5 %), but it is reasonably close to equilibrium with Opalinus Clay and will induce negligible mineralogical changes. When entering PC, the Opalinus Clay artificial pore water and displaced in situ pore water will be strongly out of equilibrium, mix with the Portland pore solution and react with the PC hydrate assemblage. If the core was initially fluid saturated, the first aliquots displaced after injection should represent the PC pore water, sampled by advective displacement [15]. If the core was only partially saturated, the early aliquots sampled may already reflect transient states of mixing and interaction, with details depending on the presence of preferential flow paths and other heterogeneities.

3.4.2. Estimation of the concrete pore solution

For the same PC composition, a paste sample was kept in a closed system. After 9 years, a part of the sample was squeezed to analysis the pore solution and crushed to carry out solid characterisation [9]. Analysis of the pore solution is given in Table 5 and contained 200 mmol/L K and 90 mmol/L Na with a pH of 13.5. TGA and XRD revealed the presence of portlandite, C-S-H, ettringite, monocarbonate and hydrotalcite [9].

Table 5
Pore solution chemistry and saturation indices (SI) for the isolated 9-year-old hydrated PC paste from [9], the leaching experiment and the suggested pore solution for this study. Analytical error ± 10 %. Bold lines correspond to the experimental observation of the phases in the cement matrix.

	Laboratory after 9 years	Leaching experiment	Estimated pore solution
	Chemical composition (mmol/L)		
Ca	0.7	20	40
Na	91	10	75[a]
K	200	7	35.4
Cl		30	153
NO3		0.35	1.8
SO4	6.6	0.07	0.3
Si	0.05	0.01	0.05
Mg[b]	<0.001	<0.0001	<0.001
Al[b]	0.16	Not measured	0.1
pH	13.5	12.4	12.5
	Saturation indices		
CSH	**−0.1**	**−0.1**	**0.1**
ettringite	**0**	**0**	**0**
AFm- SO4	−0.1	0.1	0.2
AFm- NO3	−0.1	0	0
Friedel's salts	−0.1	0	0
Kuzel's salts	−0.1	0	0
Portlandite	**0**	**−0.1**	**0**
Anhydrite	−0.5	−0.4	−0.3
Gypsum	−0.2	−0.2	−0.1
Hydrotalcite[b]	**0**	**0**	**0**

[a] Na concentration was slightly increased in order to reach electronegativity of the solution.

[b] Mg and Al set to 0.00001 and 0.1 mmol/L for the saturation index calculations, values to match SI = ettringite.

Table 4
Measured concentrations in the Opalinus Clay artificial pore water (results obtained by ion chromatography, ICP-OES and PICARRO instrument, errors ±5 %, traced with deuterium).

pH	Na	K	Ca	Mg	*Sr*	Cl	SO_4	δ^2H_{OPA}	$\delta^{18}O_{OPA}$
				mmol/L				‰ vs. VSMOW	‰ vs. VSMOW
7.3	250.28	1.46	14.14	16.25	0.52	275.14	13.41	130.42	−11.14

However, the pore solution of the 10-year-old concrete at 1–5 cm of the interface is expected to be significantly different from the pore solution measured in a closed-system 9-year-old paste due to exchange with OPA pore water with a lower pH and different composition A sample of the same concrete emplaced in the CI experiment was chosen and taken at approximately 4–5 cm distance from the interface (Fig. S 1). The material is outside the range of visible direct interaction with OPA (usually few mm to cm [6–8]) and represents the reference for aged Portland concrete. XRD and TGA data (Fig. S 2) showed, in addition of aggregate, the presence of portlandite, ettringite, monocarbonate and hydrotalcite and indicated the presence of C-S-H. The presence of a hydrotalcite-like phase was consistent with the relatively high MgO content of 5 wt% in the unhydrated PC [8]. Possibly also AFm phases as hemicarbonate and monocarbonate could be present, but due to the broad XRD signal they could not be distinguished from the reflections of the hydrotalcite.

Leaching experiments on the same sample helped to estimate the pore solution of the concrete. The leaching experiment (Table 4) showed a rather low pH of about 12.3 and a calcium concentration lower than expected at saturation with Portlandite. The measured concentrations correspond mostly to the leached ions diluted by the applied solid/liquid ratio and back calculations to pore water concentrations was required to estimate the pore solution composition. For simple back calculations, the NaCl and KCl were considered as non-desorbed from the solids and the measurement corresponds more or less to the NaCl and KCl only present in the pore solution. The OH concentration (i.e. pH) and the Ca concentration are controlled by the equilibrium with Portlandite as it is the main phase buffering the pH. Hence, the concentration of Ca was estimated from the solubility curve of portlandite at the given pH instead of using a dilution factor. Additionally, the *Al* was not measured, but *Al* concentration usually decreases with a pH decrease. The estimated *Al* concentration was set to be at equilibrium with ettringite and hydrotalcite. The estimated pore solution is given in Table 5.

The concentrations of Na^+ and K^+ in the leached solutions ($\neq$ estimated pore solutions) are very similar, about 10 mmol/L and 7 mmol/L, respectively. The Cl concentration was about 30 mmol/L, almost double compared to the Na + K concentration (10 + 7 mmol/L). The concentration of SO_4^{2-} (0.07 mmol/L) is lower than the NO_3^- concentration (0.35 mmol/L), certainly due to the initial presence of an additive containing NO_3^- and the usual precipitation of SO_4^{2-} in ettringite and AFm phases. Anion as Cl^- and NO_3^- are supposedly precipitated in the LDH phases, either as AFm phases like Friedel's and/or Kuzel's salts or as hydrotalcite-like phases (as detailed in 3.1.2). The latter are usually sorbed in the interlayer of the LDH when concretes are in contact with saline water, i.e. dissolved $Cl^- > 550$ mmol/L [42] and are loosely bound. Friedel's salts have been observed even for lower concentrations [43,44].

The estimated pore solution contained a relatively high dissolved Cl concentration (153 mmol/L) compared to a normal Portland cement pore solution indicating that there were exchanges between the concrete and the OPA and no clogging occurred. This is due to the infiltration of the OPA pore water. Interestingly, the content of sodium was rather low (75 mmol/L), compared to the normal Portland cement pore solution (91 mmol/L) or the OPA pore water (250 mmol/L) indicating a strong sorption to the cement hydrates and/or precipitation in new phases.

The saturation indices were calculated (Table 5) in order to compare the pore solution of the closed-system paste from [9] and the estimated pore solution of the in-situ enriched paste/mortar (this study). The main hydrates (portlandite, C-S-H, ettringite, and hydrotalcite) have SI values close to 0 ± 0.1, confirming that the solutions were nearly at equilibrium. Interestingly, the pore solution is undersaturated with respect to anhydrite and gypsum. The high concentration of Cl caused the solution to be nearly at equilibrium with respect to Fridel's, and Kuzel's salts. It is also possible that Cl slightly adsorbed on C-S-H. Finally, the pore solution was at equilibrium with NO_3-AFm due to the large quantities of NO_3^- measured.

While the direct interface (first few millimetres) of the OPA/PC is usually studied, the SEM/EDS results and the leaching experiments showed changes in the concrete also at approx. 5 cm of the interface, outside the range of visible zonation/alteration:

- Ingress of some components of Opalinus Clay pore water into the concrete
- Large amount of Cl^- in the pore solution associated with some uptake in the solids
- Depletion of K^+, in the pore water of the concrete probably due to the migration into the OPA and/or precipitation in new phases
- Depletion of Na^+, in the pore water of the concrete probably due to the precipitation in new phases, supposedly associated with a decreased pH

3.4.3. *Exfiltrating aliquots*

The concentrations of dissolved ions measured over time are presented in Fig. 11 and the result of the full analyses is given in Table S 2 (pH, ion concentrations, total organic carbon, total inorganic carbon,

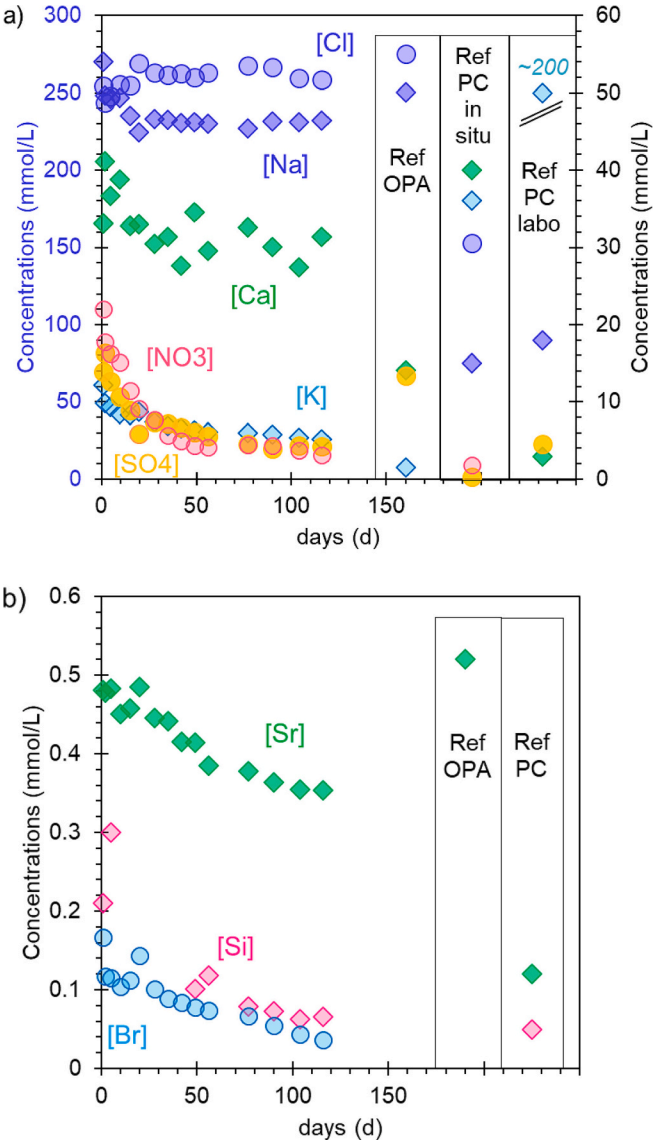

Fig. 11. a) Dissolved Na, Cl (left blue axis), Ca, NO_3, K and SO_4 (right black axis), & b) dissolved Sr, Br, Si measured in the aliquots over time (ref PC corresponds to the data given in [9]). (For interpretation of the references to colour in this figure legend, the reader is referred to the web version of this article.)

dissolved organic carbon, δ^2H, $\delta^{18}O$ and calculated saturation indices for the relevant cement phases).

The composition of the aliquots over time differed strongly from the OPA pore water injected or the estimated pore solution of the concrete (Fig. 11). The sodium and chloride concentrations remained between 270 and 230 mmol/L and 254 and 260 mmol/L, respectively, close to the artificial pore water composition for Cl, and somewhat reduced for Na. The sodium concentration at early time was 270 mmol/L and decreased to a level of 230 ± 3 mmol/L after 20 days. It is likely that during the first day the joint system in the OPA let the artificial pore water through, flooding the interface region and that the fluid did not equilibrate with the PC that contained much lower levels of Na and Cl (~75 and 150 mmol/L respectively, see Table 5). The first aliquots presented pH lower than 12.5 and a large content of dissolved organic carbon. Due to the low pH, the aliquots were undersaturated with most of the cement hydrates, especially undersaturated with respect to portlandite (Table S 2). After 10 days, a pH of 12.5 (indicative of buffering by portlandite) and a lower content of organics were measured.

This suggested a very early partial breakthrough of the major charge-carriers during the earliest phase when also much gas was expelled attesting to elevated volumetric flow rates (Fig. 10). This also suggests that there were likely also preferential pathways in the PC and thus an inability to substantially buffer the injected OPA pore fluid when fluxes were high.

Similarly to the organics, the concentration of potassium decreased from 12 to 5 mmol/L with time, a value well above the injected OPA pore water but also well below the expected pore water in PC. Some K was apparently taken up by the fluid travelling through PC, perhaps from an inventory of K associated with C-S-H. This was continuously depleted as K was washed out and less K was present in the system. As mentioned above, K is also involved in cation exchange in OPA. The concentration of calcium in solution remained more or less constant and the SI calculated for the portlandite indicated that the aliquots were all at equilibrium with respect portlandite due to the portlandite buffer. A decrease in dissolved calcium and pH is expected only after the total dissolution of portlandite.

Strontium elutes initially at concentrations close to the injected fluid, and was gradually decreasing by uptake of some *Sr* in the PC. Substantial nitrate, not present in the OPA clay artificial pore water, was measured (~20 mmol/L) initially, decreasing with time. This corresponds to the leaching of the nitrate present as initial additive in the PC pore solution and/or incorporated in the LDH, mono-sulphate or mono-carbonate hydrates, and mobilised by high Cl concentrations. Dissolved silica (not contained in the injected fluid) initially elutes above expected values from OPA in situ conditions (ca. 0.15 mmol/L) and this is therefore mobilised from the PC, approaching expected PC pore water values with time.

The concentration of sulphate in the Opalinus Clay pore water (13–14 mmol/L) elutes initially at this concentration, decreasing with time. The decrease of SO_4^{2-} is related to the uptake by the cementitious phases, for example the precipitation of ettringite, AFm or gypsum [42,45].

Finally, bromide is not present in the initial Opalinus Clay artificial pore water and is leached from the initial pore water of Opalinus Clay (ca. 0.5 mmol/L at this location) with some loss passing through PC.

The existence of tracers commonly assumed as inert in the core sample or in the artificial pore water may allow the estimation of transport properties from their concentration evolution in the sampled aliquots. The complex and heterogeneous nature of the compound core (including an interface region) complicates or even makes data interpretation or quantitative processing impossible. First of all, the transport-active porosity strongly decreased initially, and continued to decrease throughout the entire experiment (Sections 3.2 and 3.3.3). Therefore, transient transport properties must be assumed. In addition, OPA bedding was oblique to the transport direction and the interface with a possible sealing skin that further complicates data interpretation.

The initial tracer concentrations in the porewaters of both parts of the core were speculative or unknown after 10 years of interaction with the surrounding of the Mont Terri CI experiment. And - last but not least - water tracers and anions can interact with cement hydrates, which delayed the breakthrough.

The δ^2H measured in the sampled aliquots were compared to the δ^2H_{OPA} added initially to the artificial pore water using the Eq. (6) and is presented in Fig. 12. This normalised breakthrough was equal to 0.45 in the first syringes. After 10 days, the ratio stabilised at ~0.6 and did not reached 1 after 116 days.

$$\frac{\delta^2H - \delta^2H_{OPA\_natural}}{\delta^2H_{OPA\_enriched} - \delta^2H_{OPA\_natural}} \quad (6)$$

where δ^2H is the data measured in the aliquot (Table S 2), $\delta^2H_{OPA\_natural}$ is the content of isotope measured in the natural OPA (Table S 1) and $\delta^2H_{OPA\_enriched}$ is the content measured in the enriched OPA (APW, Table 4). $\delta^{18}O$ was treated in an analogous fashion.

The anion breakthrough was also calculated from the concentration of Br measured in the aliquots. Only present in the pore water of the OPA in the core, the dissolved Br may be used as a negative breakthrough neglecting the possible uptake of Br^- into cement phases, following the Eq. (7):

$$\frac{[Br]_{initial} - [Br]}{[Br]_{initial}} \quad (7)$$

where $[Br]$ is the Br concentration measured in the aliquot (Table S 2) and $[Br]_{initial}$ is the concentration of Br measured in the natural OPA (Table S 1).

The normalised breakthrough of Br (Fig. 12) reached 0.6 after one day, and was close to 1 after 116 days, meaning a complete (negative) breakthrough was almost reached. The breakthrough of a non-reactive anionic tracer in an advection-diffusion regime is faster than a water tracer in OPA due to the effect of anion-exclusion by negatively-charged clay mineral surfaces [15]. The shape of the breakthrough curve for Br is however not that of a non-reactive tracer and indicates that initially some Br was retained in the PC. The initial jump to a partial breakthrough already during the sampling period for the first syringe indicates the afore mentioned fast imbibition of the joint system and initially unsaturated porosity.

The main difficulty in interpreting the δ^2H breakthrough relates to

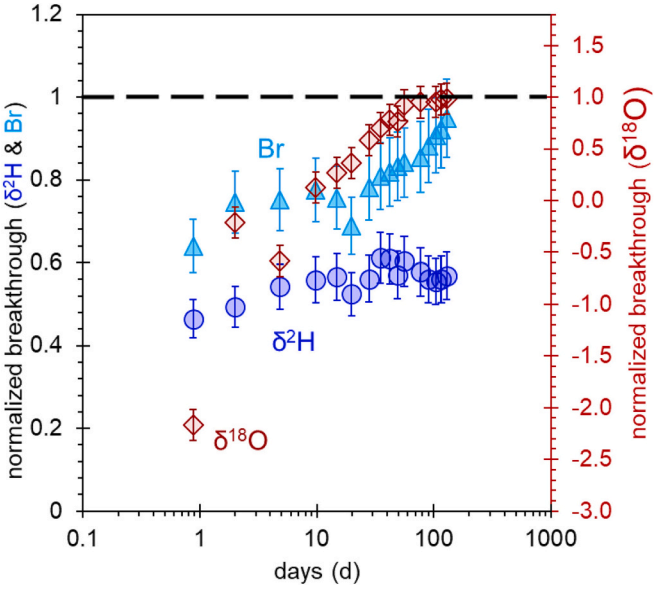

Fig. 12. Normalised breakthrough measured in the aliquots over time. δ^2H and $\delta^{18}O$: normal breakthroughs, Br-: negative breakthrough.

the unknown isotopic composition in the PC pore water, and the extent that cement hydrate assemblage may interact isotopically at this time scale. Assuming that PC has an initial signature similar to tap water (−55 to −65 ‰VSMOW) or perhaps even lighter due to hydrate formation, one observes qualitatively the same initial rapid partial breakthrough as with Br, with a fast initial surge of tracer already present in the first syringe. Larger pores along some better-connected zones in the concrete, partially not saturated initially (see Section 3.3.2), provide preferential pathways for advective transport of pore water coming from the OPA side. The breakthrough is slowly progressing under a regime of decreasing advection. Diffusive interaction between the pathways and the cement matrix pore water (e.g., capillary pores, less affected by advection) leads to a mixing of the two isotope signals, with increasing PC influence when advection slows down. There is almost no progress in breakthrough after 10 days, and this may be due to an effective retention of the deuterium signal by the PC (interaction with cement hydrates), more so than could be explained by mixing of pore waters. Note that the breakthrough scale is defined relative to the known isotopic composition the Opalinus Clay, and a breakthrough in pure Opalinus Clay would evolve in a smooth sigmoidal shape from a value of 0 to 1. Fig. 12 emphasises the effect of PC on the breakthrough, but it is also affected by a rapid initial ingress of the synthetic pore water.

The same is true for the breakthrough of $\delta^{18}O$ that shows a large scatter in the first three aliquots that plot as negative points on the breakthrough normalised to a value of the Opalinus Clay pore water. The reason for this scatter is not understood. Thereafter, the breakthrough is progressing towards the concentration of the injected pore water. Again, a more detailed interpretation – e.g. concerning also the different behaviour of $\delta^{2}H$ and $\delta^{18}O$ - is difficult in the absence of a constraint on the initial isotopic ratios in the PC (after 10 years of exposure next to Opalinus Clay).

All breakthrough curves share an asymmetric breakthrough with a very steep initial increase. Early transport is advection controlled, with fracture flow in the OPA and diffusive matrix exchange. A very rough assessment of Péclet numbers based on the observed flowrates (calculated from Table S2) and generic diffusion and porosity properties of OPA or concrete results in an early value around 1. The subsequent tailing of the values indicates a transition towards hydrodynamic dispersion with diffusion, in line with a decrease in Péclet number. The limitations mentioned above make further quantitative interpretation impossible.

4. Conclusions

The long-term isolation properties of a geological facility for deep storage of nuclear waste rely on the stability of the geological environment and the engineered barrier systems. Particularly the properties of the interfacial zones between different cementitious and clay materials may affect the overall performance. Here, we tested a concrete/claystone interface that previously aged for 10 years under relevant conditions and developed a small-scale multiply-zoned mineral alteration region, more prominent in the PC matrix than in the Opalinus Clay. Pre-existing bedding-parallel jointing oriented oblique to the interface, and partial de-saturation during sample preparation and storage render this an analogue of an excavation-disturbed zone in contact with a Portland cement material. A cylindrical compound sample with 50 mm diameter contained this complex interface and was subjected to a large hydraulic head gradient (40 m/m) injecting a synthetic clay-equilibrated pore water into the Opalinus Clay part, across the interface and through the PC part to sampling by syringes. An immediate breakthrough of the main fluid components Na-Cl, sulphate, deuterated water and the inert tracer bromide attested rapid initial transport along the partially open joint system, across the interface, and likely along preferential flow paths through PC. A cement-signature in the outflow was evident by Ca elution and elevated pH with approximate portlandite buffering, and elevated concentrations of K, Si and nitrate (from additives). This initial rapid flooding was accompanied by gas displacement from the unsaturated pore space, but also some induced gas production, supposedly by microbial activity. Hydraulic conductivity was rapidly decreasing as the joint system was self-sealing, and so were average flow velocities (residence time) and the hydraulic conductivity was approaching a value not much above a value for undisturbed shaley facies of Opalinus Clay parallel to bedding. At the end of chemical monitoring (116 days), the chemical composition of the outflow was still evolving towards a more PC-influenced pore water, but superimposed with a continuous elution of the high Na-Cl salinity of the synthetic OPA-type injection fluid.

It was not possible to quantify the effect that the characterised mineralogical alteration zone at the interface may have played– the hydraulics were dominated by a disturbed state that likely also disrupted any continuous skin that may have been present before opening of joints. Note that such a disturbed state is not expected to be present at saturated in situ conditions – interface samples from several campaigns invariably attested cohesion across the interface including also thin alteration zones with reduced porosity [7–9,14]. A companion hydraulic experiment with a less-aged mortar (3 years plus 2 years cold storage) from the same field experiment and an interface oriented parallel to bedding did show a low bulk hydraulic conductivity that suggest a potential thin skin acting as a barrier (partial data published in [40,41]).

For the first time the pore solution of the concrete at few centimetres away from the interface with OPA (~5 cm) was estimated. It showed a large content of dissolved Cl, and relatively high dissolved SO_4 and NO_3. Calculated OH concentration based on electronegativity indicates that the pH was rather low, only to let the solution at equilibrium with portlandite (i.e. ~12.5) indicating a modified concrete after 10 years. This might affect the sorption and diffusion properties of such concrete after several years. The sorption of this specific concrete was studied in [46] in order to give updated sorption values to directly examine the transport effects of such interfaces at the field scale by a diffusion experiment with appropriate tracers (^{3}H, ^{36}Cl, for example), and examine subsequently tracer profiles across the interface (e.g. CI-D experiment at the Mont Terri rock laboratory).

The novel experimental approach combined hydraulic testing and chemical monitoring with many repeat X-ray CT scans while the experiment was autonomously running. This greatly improved our process understanding, mainly via a semi-quantitative documentation of volumetric and textural incremental changes. The self-sealing properties of Opalinus Clay (closing of joints) were directly observed for the first time.

The observations in this experiment indicate that initial flow across the EDZ of OPA that has previously interacted with cement, is relatively fast and not hindered by a skin at the cement-clay interface. With ongoing hydration, swelling of the OPA and of the potentially present buffer material (e.g., bentonite), the flow rate decreases. The OPA pore water crosses the OPA-cement interface and the cement liner and enters the buffer. The cement signature of this water, especially pH, increases with decreasing flow. Now, the influence of the skin at the cement-OPA interface on transport might increase again, and cement-OPA interaction might continue. Further CT investigations on the core still subjected to artificial pore water infiltration, or a post mortem analysis of the core, might elucidate these processes.

The interaction of the infiltrating artificial pore water with OPA and cement strongly depends on the transport regime, which changes during the experiment from fast-advective along preferential pathways to a low flow expected in OPA with an increasing significance of diffusion. This makes it impossible to unambiguously derive all interaction mechanisms of the different solutes with both materials from the exfiltrating aliquot compositions without a detailed reactive transport modelling exercise. Especially the interactions of the water tracers with cement remain speculative. The flattening of the deuterium breakthrough at 0.6 disqualifies its use as non-reactive tracer in cement, and the slower Br breakthrough compared to $\delta^{18}O$ confirms the well-known anion

retention in cement. Both types of interactions are not reported for OPA [18]. Nevertheless, the exfiltrating chemistries indicate the degree of interaction during the different flow regimes.

More experimental work on the transport could be done, as e.g. with positron-emission tomography (PET) to directly image the mobile phase in 3D, and its time evolution of such heterogeneous interface [47].

CRediT authorship contribution statement

Ellina Bernard: Investigation, Acquisition of data, Analysis and interpretation of data, Writing – original draft, Writing – review & editing, Visualisation. **Andreas Jenni:** Investigation, Analysis and interpretation of data, Writing – review & editing. **Nikolajs Toropovs:** Writing – review & editing, Visualization. **Urs Mäder:** Conception and design of study, Analysis and interpretation of data, Investigation, Writing – original draft, Writing – review & editing, Visualisation, Supervision.

Declaration of competing interest

The authors declare that they have no known competing financial interests or personal relationships that could have appeared to influence the work reported in this paper.

Data availability

Data will be made available on request.

Acknowledgment

The research leading to these results has received funding from the European Union's Horizon 2020 Research and Training Programme of the European Atomic Energy Community (EURATOM) (H2020-NFRP-2014/2015) under grant agreement n° 662147 (CEBAMA). The CI Project of the Mont Terri rock laboratory kindly shared data and funded the sampling campaign (financed by ANDRA, CRIEPI, FANC, Nagra, NWMO, Obayashi, RWS, SCK-CEN). Christoph Neururer, Anneleen Foubert (both at the University of Fribourg, Switzerland) supported the X-ray CT data acquisition on the Bruker Skyscan 2211 instrument at the University of Fribourg (Swiss National Science Foundation R'EQUIP Grant n° 150731). We would like to thank Michele Griffa and Beat Münch (both at Empa) for the helpful discussions on treatment of image analyses.

Appendix A. Supplementary data

Supplementary data to this article can be found online at https://doi.org/10.1016/j.cemconres.2023.107180.

References

[1] NAGRA, Demonstration of Feasibility of Disposal ("Entsorgungsnachweis") for Spent Fuel, Vitrified High-level Waste and Long-lived Intermediate-level Waste, Opalinus Clay Project, 2002.
[2] ANDRA, Evaluation of the feasibility of a geological repository in an argillaceous formation, in: Collection Les rapports 2005, 2005.
[3] SCK•CEN, Preparatory Safety Assessment. Conceptual Model Description of the Reference Case, ER-215, CCHO - 2009-00940000, SCK•CEN, Mol, Belgium, 2012.
[4] I. Techer, D. Bartier, P. Boulvais, E. Tinseau, K. Suchorski, J. Cabrera, A. Dauzères, Tracing interactions between natural argillites and hyper-alkaline fluids from engineered cement paste and concrete: chemical and isotopic monitoring of a 15-years old deep-disposal analogue, Appl. Geochem. 27 (2012) 1384–1402.
[5] D. Bartier, I. Techer, A. Dauzères, P. Boulvais, M.-M. Blanc-Valleron, J. Cabrera, In situ investigations and reactive transport modelling of cement paste/argillite interactions in a saturated context and outside an excavated disturbed zone, Appl. Geochem. 31 (2013) 94–108.
[6] E. Bernard, A. Jenni, M. Fisch, D. Grolimund, U. Mäder, Micro-X-ray diffraction and chemical mapping of aged interfaces between cement pastes and opalinus clay, Appl. Geochem. 115 (2020), 104538.
[7] A. Jenni, T. Gimmi, P. Alt-Epping, U. Mäder, V. Cloet, Interaction of ordinary Portland cement and Opalinus Clay: Dual porosity modelling compared to experimental data, Phys. Chem. Earth, Parts A/B/C 99 (2017) 22–37.
[8] A. Jenni, U. Mäder, C. Lerouge, S. Gaboreau, B. Schwyn, In situ interaction between different concretes and Opalinus clay, Phys. Chem. Earth, Parts A/B/C 70 (2014) 71–83.
[9] U. Mäder, A. Jenni, C. Lerouge, S. Gaboreau, S. Miyoshi, Y. Kimura, V. Cloet, M. Fukaya, F. Claret, T. Otake, M. Shibata, B. Lothenbach, 5-year chemico-physical evolution of concrete-claystone interfaces, Swiss J. Geosci. 110 (2017) 307–327.
[10] A. Dauzères, G. Achiedo, D. Nied, E. Bernard, S. Alahrache, B. Lothenbach, Magnesium perturbation in low-pH concretes placed in clayey environment - solid characterizations and modeling, Cem. Concr. Res. 79 (2016) 137–150.
[11] C. Lerouge, S. Gaboreau, S. Grangeon, F. Claret, F. Warmont, A. Jenni, V. Cloet, U. Mäder, In situ interactions between opalinus clay and low alkali concrete, Phys. Chem. Earth, Parts A/B/C 99 (2017) 3–21.
[12] S. Gaboreau, C. Lerouge, S. Dewonck, Y. Linard, X. Bourbon, C. Fialips, A. Mazurier, D. Prêt, D. Borschneck, V. Montouillout, In-situ interaction of cement paste and shotcrete with claystones in a deep disposal context, Am. J. Sci. 312 (2012) 314–356.
[13] S. Gaboreau, D. Prêt, E. Tinseau, F. Claret, D. Pellegrini, D. Stammose, 15 years of in situ cement–argillite interaction from Tournemire URL: characterisation of the multi-scale spatial heterogeneities of pore space evolution, Appl. Geochem. 26 (2011) 2159–2171.
[14] P. Lalan, A. Dauzères, L. De Windt, J. Sammaljärvi, D. Bartier, I. Techer, V. Detilleux, M. Siitari-Kauppi, Mineralogical and microstructural evolution of Portland cement paste/argillite interfaces at 70° C-considerations for diffusion and porosity properties, Cem. Concr. Res. 115 (2019) 414–425.
[15] U. Mäder, Advective displacement method for the characterisation of pore water chemistry and transport properties in claystone, Geofluids 2018 (2018).
[16] F.J. Pearson, D. Arcos, A. Bath, J.-Y. Boisson, A.M. Fernandez, H.-E. Gäbler, E. Gaucher, A. Gautschi, L. Griffault, P. Hernan, H.N. Waber, in: Mont-Terri Project – Geochemistry of Water in the Opalinus Clay Formation at the Mont Terri Rock Laboratory, Reports of the FOWG, Geology Series 5, 2003, p. 319.
[17] E. Wieland, B. Lothenbach, M. Glaus, T. Thoenen, B. Schwyn, Influence of superplasticizer on the long-term properties of cements and possible impacts on radionuclide uptake in cement based repository for radioactive waste, Appl. Geochem. 49 (2014) 126–142.
[18] S. Klein, M. Staring, K. Murphy, M.A. Viergever, J.P. Pluim, Elastix: a toolbox for intensity-based medical image registration, IEEE Trans. Med. Imaging 29 (2009) 196–205.
[19] P. Wersin, M. Pekala, M. Mazurek, T. Gimmi, U. Mäder, A. Jenni, D. Rufer, A. L., NTB 18-01, Porewater Chemistry of Opalinus Clay: Methods, Data, Modelling & Buffering Capacity, 2021.
[20] U. Mäder, TECHNICAL NOTE 2015-128, CI (Cement Clay Interaction) Experiment: Sampling and Analysis of Opalinus Clay Pore Water From Test Interval BCI-4 (2015/2016), 2018.
[21] U.K. Mäder, Reference Pore Water for the Opalinus Clay and "Brown Dogger" for the Provisional Safety-analysis in the Framework of the Sectoral Plan - Interim Results(SGT-ZE), Arbeitsbericht NAB 09-14, 2009.
[22] D. Kulik, T. Wagner, S.V. Dmytrieva, G. Kosakowski, F. Hingerl, K.V. Chudnenko, U. Berner, GEM-selektor geochemical modeling package: revised algorithm and GEMS3K numerical kernel for coupled simulation codes, Comput.Geochem. 17 (2013) 1–24.
[23] T. Thoenen, W. Hummel, U. Berner, E. Curti, The PSI/Nagra Chemical Thermodynamic Database 12/07, PSI report 14-04, Villigen PSI, Switzerland, 2014.
[24] B. Lothenbach, D.A. Kulik, T. Matschei, M. Balonis, L. Baquerizo, B. Dilnesa, G. D. Miron, R.J. Myers, Cemdata18: a chemical thermodynamic database for hydrated Portland cements and alkali-activated materials, Cem. Concr. Res. 115 (2019) 472–506.
[25] C. Nussbaum, A. Kloppenburg, T. Caër, P. Bossart, in: Tectonic Evolution Around the Mont Terri Rock Laboratory, Northwestern Swiss Jura: Constraints From Kinematic Forward Modelling, Mont Terri Rock Laboratory, 20 Years, Springer, 2018, pp. 41–68.
[26] B. Ma, B. Lothenbach, Thermodynamic study of cement/rock interactions using experimentally generated solubility data of zeolites, Cem. Concr. Res. 135 (2020), 106149.
[27] B. Lothenbach, A. Nonat, Calcium silicate hydrates: solid and liquid phase composition, Cem. Concr. Res. 78 (2015) 57–70.
[28] M. Balonis, B. Lothenbach, G. Le Saout, F.P. Glasser, Impact of chloride on the mineralogy of hydrated Portland cement systems, Cem. Concr. Res. 40 (2010) 1009–1022.
[29] A. Machner, M. Zajac, M.B. Haha, K.O. Kjellsen, M.R. Geiker, K. De Weerdt, Chloride-binding capacity of hydrotalcite in cement pastes containing dolomite and metakaolin, Cem. Concr. Res. 107 (2018) 163–181.
[30] G. Plusquellec, A. Nonat, Interactions between calcium silicate hydrate (CSH) and calcium chloride, bromide and nitrate, Cem. Concr. Res. 90 (2016) 89–96.
[31] K. De Weerdt, A. Colombo, L. Coppola, H. Justnes, M.R. Geiker, Impact of the associated cation on chloride binding of Portland cement paste, Cem. Concr. Res. 68 (2015) 196–202.
[32] E. Bernard, Y. Yan, B. Lothenbach, Effective cation exchange capacity of calcium silicate hydrates (CSH), Cem. Concr. Res. 143 (2021), 106393.
[33] J. Haas, A. Nonat, From C-S–H to C–A–S–H: experimental study and thermodynamic modelling, Cem. Concr. Res. 68 (2015) 124–138.

[34] C. Labbez, A. Nonat, I. Pochard, B. Jönsson, Experimental and theoretical evidence of overcharging of calcium silicate hydrate, J. Colloid Interface Sci. 309 (2007) 303–307.
[35] P. Bossart, F. Bernier, J. Birkholzer, C. Bruggeman, P. Connolly, S. Dewonck, M. Fukaya, M. Herfort, M. Jensen, J.-M. Matray, Mont Terri rock laboratory, 20 years of research: introduction, site characteristics and overview of experiments, Swiss J. Geosci. 110 (2017) 3–22.
[36] T. Gimmi, O.X. Leupin, J. Eikenberg, M.A. Glaus, L.R. Van Loon, H.N. Waber, P. Wersin, H.A. Wang, D. Grolimund, C.N. Borca, Anisotropic diffusion at the field scale in a 4-year multi-tracer diffusion and retention experiment–I: insights from the experimental data, Geochim. Cosmochim. Acta 125 (2014) 373–393.
[37] H.F. Taylor, Cement Chemistry, Thomas Telford London, 1997.
[38] T.C. Powers, Structure and physical properties of hardened Portland cement paste, J. Am. Ceram. Soc. 41 (1958) 1–6.
[39] F. Jacobs, Cl-Experiment: Water permeability analysis of 2 year old samples, Mont Terri Technical Note TN 2015-101, Mont Terri Project, 2015.
[40] E. Bernard, A. Jenni, U. Mäder, S. Reichenwallner, Aged Interface Between Opalinus Clay and Low-pH Mortar: Sample Characterization, X-ray Computed Tomography and Core Infiltration Experiment, Cebama, 3rd Annual Workshop, 17-18 AprilNantes (France), 2018.
[41] Cebama-D1.06, Urs Mäder (UniBern), in: Enhancements to State-of-the-art Understanding for Cement-Clay Interactions Based on CEBAMA Experimental Studies, p28, 2019, p. 34.
[42] K. De Weerdt, B. Lothenbach, M. Geiker, Comparing chloride ingress from seawater and NaCl solution in Portland cement mortar, Cem. Concr. Res. 115 (2019) 80–89.
[43] M. Saillio, V. Baroghel-Bouny, F. Barberon, Chloride binding in sound and carbonated cementitious materials with various types of binder, Constr. Build. Mater. 68 (2014) 82–91.
[44] C. Qiao, P. Suraneni, J. Weiss, Damage in cement pastes exposed to NaCl solutions, Constr. Build. Mater. 171 (2018) 120–127.
[45] W. Kunther, B. Lothenbach, K.L. Scrivener, Deterioration of mortar bars immersed in magnesium containing sulfate solutions, Mater. Struct. 46 (2013) 2003–2011.
[46] L. Nedyalkova, J. Tits, E. Bernard, E. Wieland, U. Mäder, Sorption experiments with HTO, 36-Cl, 125-I and 14-C labeled formate on aged cement matrices retrieved from long-term in-situ rock laboratory experiments, J. Adv. Concr. Technol. 19 (2021) 811–829.
[47] E. Bernard, J. Kulenkampff, A. Jenni, U. Mäder, Coupled processes across a 10-year-old clayrock/concrete interface: results of a combined X-ray CT and PET transport experiment, in: Clay Conference 2020, 2021.